FE modeling of present day tectonic stress along the San Andreas Fault zone

FE modeling of present day tectonic stress along the San Andreas Fault zone

Matrika Prasad Koirala and Daigoro Hayashi

Simulation Tectonics Laboratory Faculty of Science
University of the Ryukyus, Nishihara, Okinawa, 903-0213, Japan

Abstract

F E modeling under plane stress condition is used to analyze the state of stress in and around the San Andreas Fault (SAF) System taking whole area of California. In this study we mainly focus on the state of stress at the general seismogenic depth of 12 km, imposing elastic rheology. The purpose of the present study is to simulate the regional stress field, displacement vectors and failures. Stress perturbation due to major fault, its geometry and major branches are analyzed. Depthwise variation from 20 km to 0.5 km is considered for the fault type analysis. Series of calculations are performed with the parametrical variations of domain properties and are applied for the strong/weak SAF. All the simulated results are finally utilized for the implication of present day plate kinematics. Although in nature there is lateral and vertical variation in rheology within single domain and different domains (not considered in this study), our simulated results are comparable with the observed data. The imposed boundary condition (fixed North American plate, Pacific plate motion along N34°W vector up to northern terminus of the San Andreas faults and N50°E vector motion for the subducting Gorda and Juan de Fuca plates) had simulated the present day regional σ_{Hmax} orientation and displacement vector. Simulated results show some local effect on the stress field and displacement vector by the main strand of the fault and probably its geometry and branch (Garlock Fault). Probably the low angle σ_{Hmax} orientation to the strike of the SAF system in the South California (although there are some high angle σ_{Hmax} orientation in southeastern California) compare to the central and northern California is due to the big bend and the Garlock Fault. This modeling had also beautifully simulated the left lateral strike slip movement on the Garlock Fault. Failure analysis performed based on Byerlee's law directly test the strong SAF and variation of physical parameters in the Mohr-Coulomb failure criterion is utilized to test relatively strong/weak SAF. Our simulated results (like stress, displacement vector, and failures) in the weak fault in relatively strong crust conditions has more or less reproduced comparable and theoretically correct results, allowed us to favor weak fault in relatively strong crust. Depthwise variation of the fault type reveal that as the depth increases, the fault types are generally normal and shallow depth gives more strike slip and thrust fault. In conclusion SAF may terminate as a normal fault at the depth.

1. Introduction

The San Andreas fault (SAF) system, a complex of faults that display predominantly large-scale strike slip, is part of an even more complex system of faults, isolated segments of the East Pacific Rise, and scraps of plates lying east of the East Pacific Rise that collectively separate the North American plate from the Pacific

Received: January 16, 2009

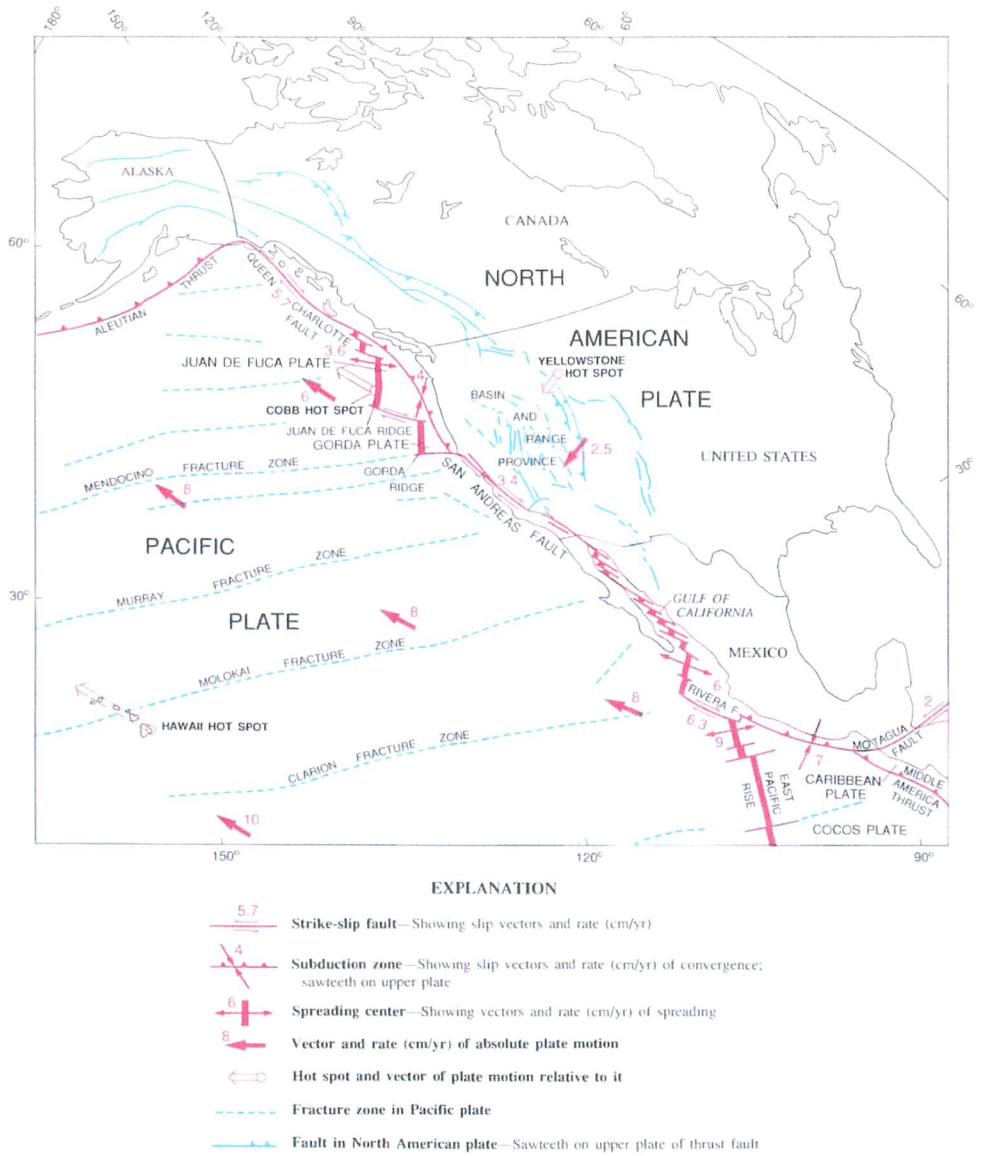

Fig.1 Cenozoic tectonic setting of the Western North America showing relation of the San Andreas Fault as one element in the complex boundary between the North American and Pacific plates (Wallace, 1990 and referenced therein)

plate (Wallace, 1990) (Fig. 1). The SAF system is a right lateral strike slip fault mainly and has many other small faults, some are left lateral some thrust and some normal. As it consists of complex nature it is termed as fault system. Present day plate kinematics of the Pacific plate and North American plate reveal that the Pacific plate is moving towards northwest with respect to North American plate. The motion of the plate is approximately 34-60 mm/yr on a N34°W vector approximately (Atwater, 1970; Minster and Jordan, 1978; De Mets et al., 1994; Argus and Gordon, 2001; Savage et al., 2004; d'Alessio et al., 2005). When, the SAF

reached at the Mendocino fracture zone in the Northern side of the California the Gorda plate and Juan de Fuca plates are subducting below the North American plates. The Juan de Fuca plate currently subducts under the North American plate with a generalized vector motion of N50°E (Swanson, 1989) and with a velocity of 30mm/yr (Noson et al., 1988). The Gorda plate subducts with a similar direction, but at an average velocity of 18mm/yr (Wood and Kienle, 1990). The convergence rates prior to 7Ma are estimated to be 70-100mm/yr (Wood and Kienle, 1990) with intermittent increases in volcanic activity suggesting that the subduction rates have also varied through time. Generally, it is said that, the state of the stress along the SAF is fault oblique compression. But it is not so simple, if it is considered as the area near to the main fault the state of stress is fault oblique compression and away from the fault, fault normal compression. It also depends on the depth where we are measuring the maximum horizontal stress. In the present study, we had calculated the stress at the seismogenic crust (12 km depth) of the whole California area and tried to analyze the result of the stress field and displacement vector. In this study we also tried to analyze the effect of fault zone, its geometry and major branch namely the Garlock fault on the stress field. For this, we use robust and powerful finite element software package (Hayashi, 2008).

The objectives of the present study are

To evaluate the state of stress along and around the SAFS

To know the stress perturbations due to the fault zone its geometry and major branch the Garlock fault on the SAF system

To know the deviation of stress field, stress orientation, failure propagation and displacement vectors with the variation of the rheology (here expressed by physical properties of the domain materials)

To know the depth wise variation of the state of stress

Implication for the strong/weak SAF

Implication for the present day plate kinematics

Plane stress, elastic, finite element models are created to analyze the state of the stress on the whole California, especially along and around the SAF system. Different domains are created in the model by the variation of the physical properties. The simplified geological map of California (Irwin, 1990) is taken as the base map (Fig. 2)

2. Geology of area around San Andreas Fault Zone

The SAF is a right-lateral strike slip fault with a strike length of over 1200 km, from northern California to the Gulf of California. Terranes on opposite sides of the fault have been displaced up to ~300 km. The fault initiated about 30 Ma and currently accommodates most relative motion between the pacific and North American plates in California (Crowell, 1952; Atwater 1970; Powell and Weldon, 1992). On its path through nearly the length of California, the SAF separates major crustal blocks (Fig. 2). In much of northern and central California, the fault is a southeast-trending boundary between the Salinian block of granitic and metamorphic rocks on the west and the Franciscan assemblage and overlying strata of the Great Valley sequence on the east. In its southerly course the fault abruptly curves eastward to cut diagonally across the Transverse Ranges, and then splays into several auxiliary faults before the main strand terminates near the

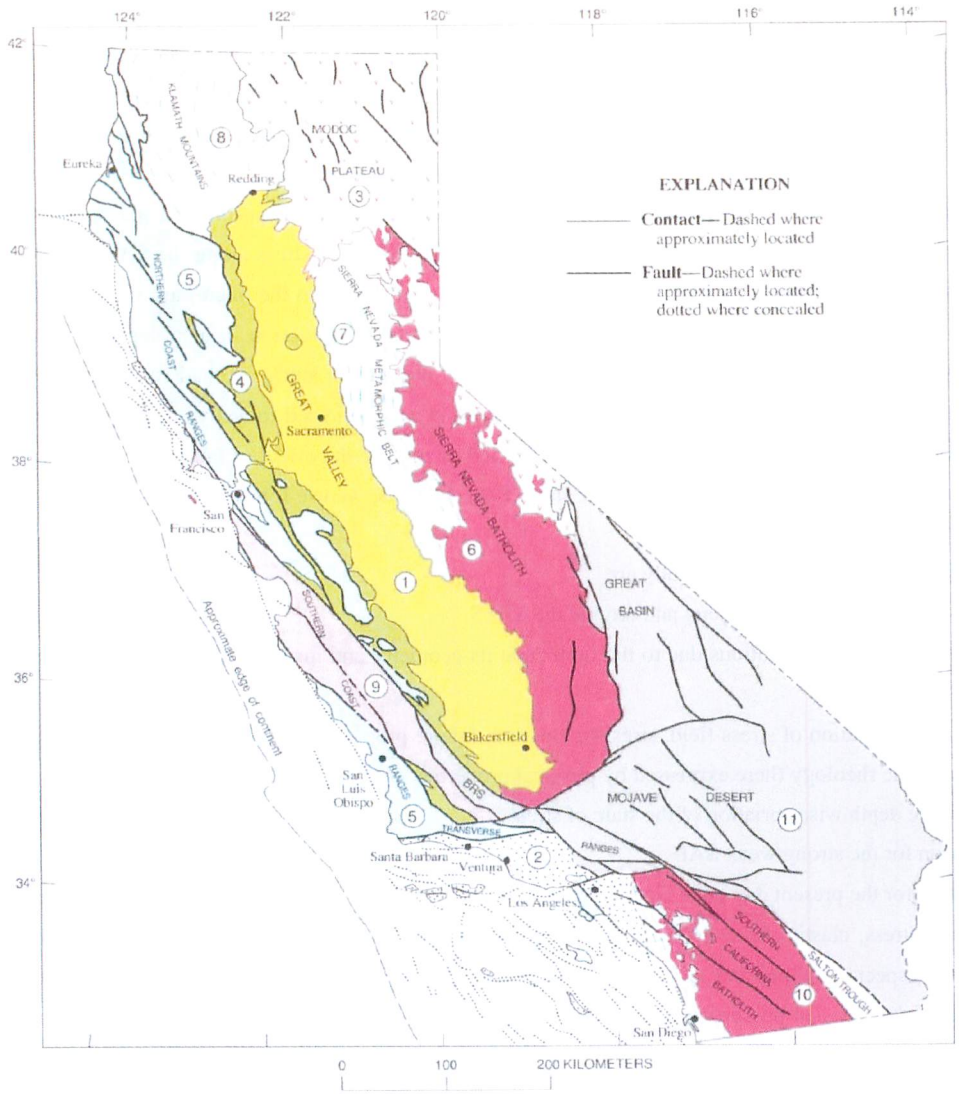

Fig. 2 Geological Sketch map of California (Irwin, 1990 and referenced therein), showing distribution of principal basement rocks. Cenozoic cover not shown except for the Modoc Plateau, northeastern Sierra Nevada, Great Valley, and Santa Barbara-Ventura Basin. Units: 1. Quaternary alluvium- shown only in Great Valley; 2. basement rocks concealed by thick Upper Cretaceous and Tertiary deposits in the Santa Barbara, Ventura, and Los Angeles Basins; 3. Cenozoic volcanic rocks of the Modoc Plateau; 4. Great Valley sequences-Lower Jurassic to Upper Cretaceous strata, including Coast Range ophiolite at the base; 5. Franciscan assemblage of Lower Jurassic to Tertiary oceanic rocks; 6. Sierra Nevada batholiths-dominantly cretaceous granitic rocks; 7. Sierra Nevada metamorphic belt-early Paleozoic to Late Jurassic rocks ,including fragments of ophiolites, island arcs, and melanges, intruded by Mesozoic plutons; 8. Klamath mountains- early Paleozoic to Late Jurassic ophiolites, island arcs, and melanges, intruded by early Paleozoic to Cretaceous plutons; 9. Salinian block-dominantly Cretaceous plutons intruding metamorphic rocks of questionable age; 10. Southern California batholiths-dominantly cretaceous plutons intruding sedimentary and volcanic rocks of Jurassic age and metamorphic rocks of mostly unknown age; 11. Mainly Precambrian metamorphic and plutonic rocks, in part overlain by Paleozoic continental shelf deposits and intruded by Mesozoic Plutons locally under thrust in southwestern part of region by schist.

Gulf of California. In southern California the basement rocks cut by the SAF are mostly Precambrian and younger metamorphic and plutonic rocks, and the crustal blocks on either side of the fault generally do not show the distinctive lithologic contrast that is so striking in central and northern California (Irwin, 1990).

3. Simulation Model

FE models are created to analyze the state of the stress on the whole California, especially along and around the SAF system. Simulation performed in this study are calculated by using the FE software package developed by Hayashi (2008).Different domains are created in the model by the variation of the physical properties. The simplified geological map of California (Fig. 2) is taken as the base map.

The FE has been used in order to solve the elastic equations and for that we have to define the geometry of the models and the correct boundary conditions to apply to it. For the FEM calculation, Young's modulus (E), Poisson ratio (υ) and density (ρ) are needed. Cohesion (c) and friction angle (ϕ) are used for the calculation of the failure. These values are selected from the available published literature (Bird and Kong, 1994; Lynch and Richards, 2001; Cai and Wang, 2001; Malservisi and Furlong, 2003; Chery et al., 2001; Parson, 2006; Flesch et al., 2007)

Elastic behavior of crust is assumed for the modeled area and this is justifiable since rheology changes from elastic to viscous at >16 km (Fuis and Mooney, 1990) depth in the study area. Realistic boundary conditions have been applied to match the natural situation that represents present day plate kinematics in the Western North America and Pacific boundary.

3.1 Model Geometry

The model covers the whole California state. The model consists of 1638 triangular elements and 879 nodes in plane stress condition. There are three types of models (A) model consisting of whole California as homogeneous single domain (B) with three domains viz. Pacific plate, North American plate and SAF zone and (C) another with the four domains consisting of the Garlock fault zone as fourth domain other three domains same as in the model (B). The Fault zone boundary is made somewhat zigzag to mimic the natural condition. Obviously the width of the fault zone is also slightly different at different places (Fig. 3).

3.2 Boundary Condition

The boundary condition imposed is representing the present day plate kinematics of the Pacific plate, remnants of the Farallon Plate and North American plate in the Western North America. In all models the displacement boundary condition is given (Fig 3). The layer west of the SAF is considered as the part of the Pacific plate and east of the San Andreas is considered as the North American plate. In the model the Pacific plate is driven by displacement vector parallel to N34°W vector and the North American plate is fixed. Fault oblique displacement is imposed progressively from 250 m, 500 m and 1000 m. In the northeastern part of the model after the San Andreas bends offshore to the Mendocino Fracture zone (Figs. 1 and 3); oblique

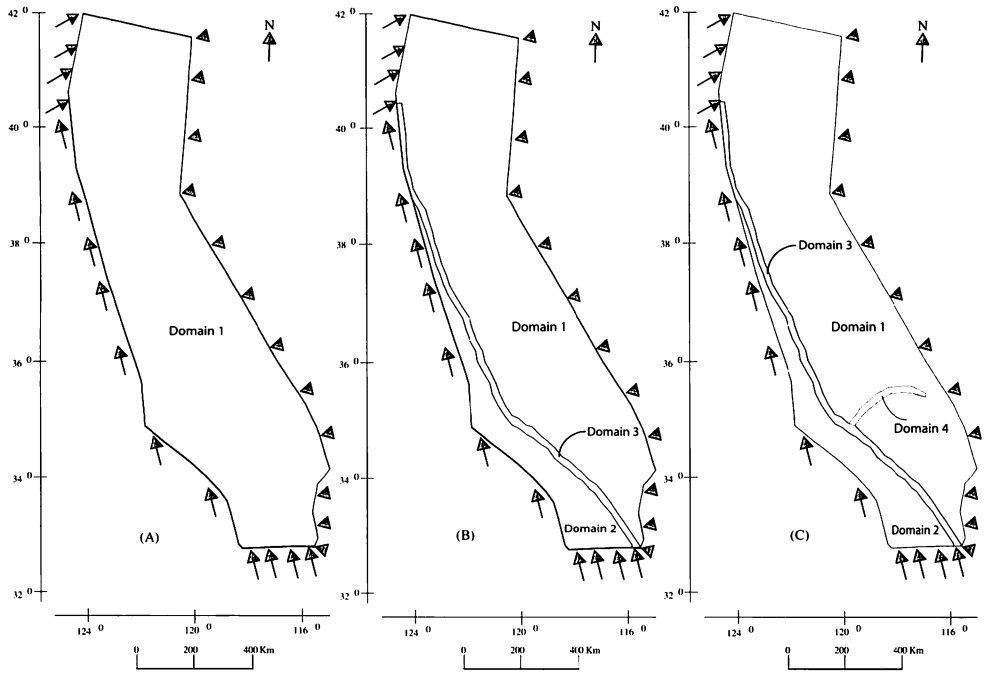

Fig. 3 Geometry and boundary condition of model, (A) Single domain model (B) three domains model and (C) four domains model

convergence boundary condition is given, where the Gorda plate and further north Juan de Fuca plate are descending below the North American plate. As the convergent rate of the Gorda plate and Juan de Fuca plate are less then Pacific plate only 60% of the displacement rate given for the Pacific plate is applied in this boundary along the N50°E vector. The northern part of the model is free to move in any direction (Fig. 3).

3.3 Rock Domain Properties

Rock domain properties, geometry, model dimension and the given displacement strongly influence the results of the numerical modeling. Selection of the suitable rock domain property is crucial. In this calculation, the model is highly simplified so that for the calculation, the properties of the upper crustal rocks are chosen according to the depth of the domain taken. The parameters taken to constraints the rock domain properties are density, Young's modulus, and Poisson's ratio. The depth of the domain is also crucial in the calculation of the modeling results. The parameters for the rock domain are taken as follows. The Pacific plate and the North American plate are simulated with a Young's modulus of 80GPa, density of 2800 kg/m^3 and a Poisson's ratio of 0.25. The fault zones are simulated with a Young's modulus of 1GPa, density of 2000 kg/m^3 and Poisson's ratio of 0.25. For all the domains the depth is considered as 12 km. For the failure analysis using Mohr-Coulomb criterion the c (cohesive strength) and ϕ (the angle of internal friction) are taken as 1 MPa (weak zone), 10 MPa (Other than weak zone) and 11° (weak zone), 30° (other than weak zone) respectively. But for the implication of depthwise variation of the failure state and fault type 20 km, 12 km, 8 km, 4 km, 1 km and

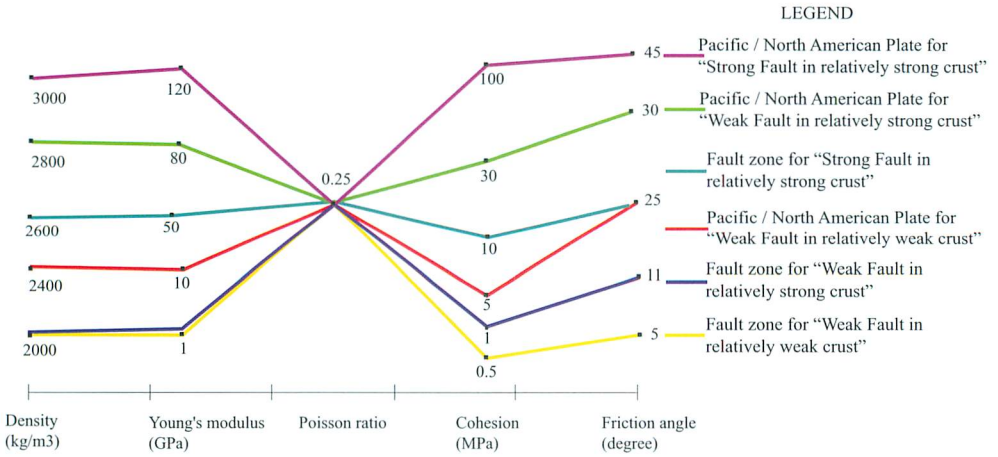

Fig. 4 Graphical presentation of the different domain properties applied for the models (A), (B) and (C).

0.5 km are also considered. We have also simulated the stress field and other parameters like σ_{Hmax}, failure and displacement vector with the variation of the physical properties for the implication of strong/weak SAF. The complete lists of parameters used for the simulation are shown in Table 1 and Fig. 4. These parameters are separated in to three groups namely "Weak fault in relatively strong crust (WFS)", "Strong fault in relatively strong crust (SFS)" and "Weak fault in relatively weak crust (WFW)".

Strength	Depth (Km)	Physical Properties					Domain
		Poison' s Ratio	Density (Kg/m^3)	Young's Modulus (GPa)	Cohesion (Mpa)	Friction angle(°)	
Weak fault in relatively strong crust	20,12,8,4,1,0.5	0.25	2800	80	30	30	Pacific Plate
		0.25	2800	80	30	30	North American Plate
		0.25	2000	1	1	11	San Andreas and other fault zone
Strong fault in relatively strong crust	20,12,8,4,1,0.5	0.25	3000	120	100	45	Pacific Plate
		0.25	3000	120	100	45	North American Plate
		0.25	2600	50	10	25	San Andreas and other fault zone
Weak fault in relatively weak crust	20,12,8,4,1,0.5	0.25	2400	10	5	25	Pacific Plate
		0.25	2400	10	5	25	North American Plate
		0.25	2000	1	0.5	5	San Andreas and other fault zone

Table 1: Physical properties of the different domains applied for the models (A), (B) and (C).

4. Modeling results

As discussed above the simulation of the California is based on the simplified geological map. Three models are created as mentioned above and the general properties of the upper crustal layer are taken to constraint the elastic models. Fault oblique progressive displacement is given in all models as mentioned already. In all the models the gravity is taken into account.

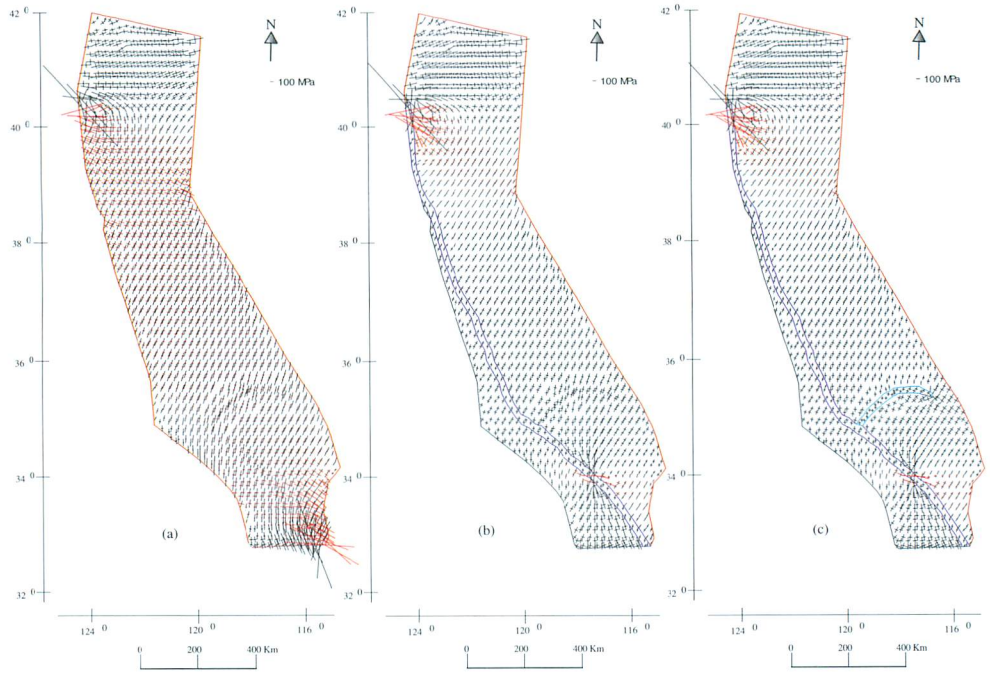

Fig. 5 Stress distribution at 1000m displacement for models (A), (B), and (C) respectively (considering weak fault in relatively strong crust), each pair of perpendicular lines represents σ Hmax (long lines) σ Hmin (short lines) in the stress field, and red bar shows the tension.

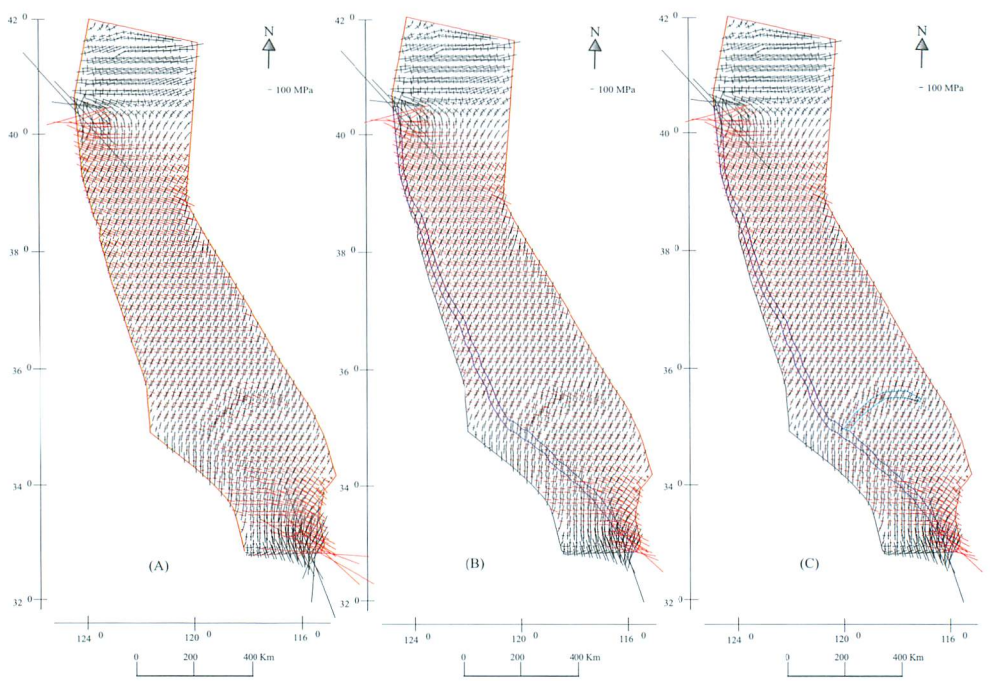

Fig. 6 Stress distribution at 1000m displacement for models (A), (B), and (C) respectively (considering strong fault in relatively strong fault), each pair of perpendicular lines represents σ Hmax (long lines) σ Hmin (short lines) in the stress field, and red bar shows the tension.

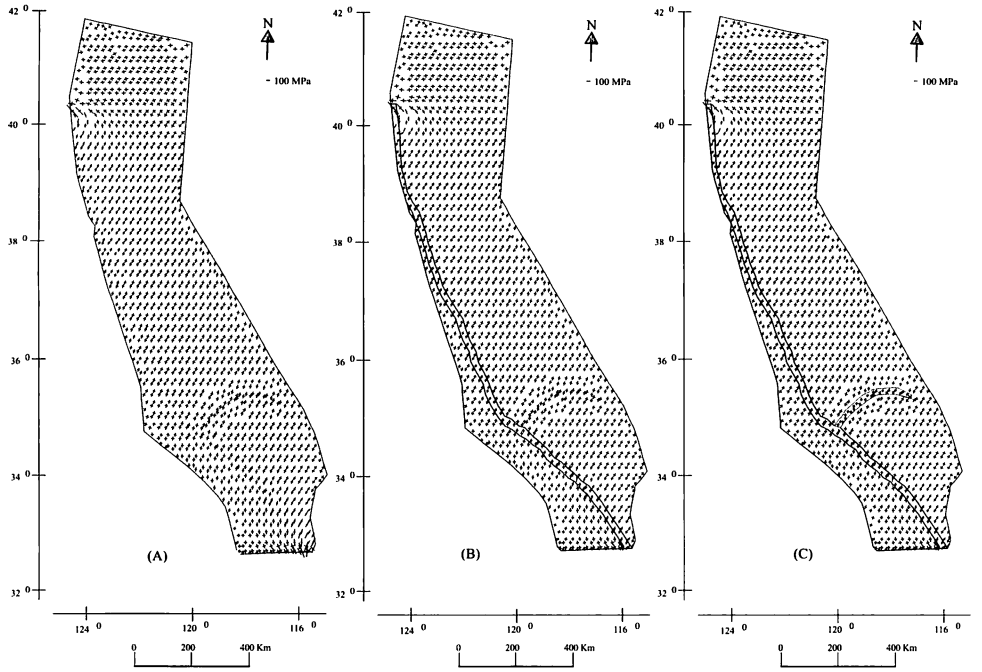

Fig. 7 Stress distribution at 1000m displacement for models (A), (B), and (C) respectively (considering weak fault in relatively weak fault), each pair of perpendicular lines represents σ Hmax (long lines) σ Hmin (short lines) in the stress field, and red bar shows the tension.

4.1 Stress field

Stress field for the three models with increasing displacements (250 m, 500 m and 1000 m) and for three sets of parametrical conditions (WFS, SFS, WFW) are calculated. Figs. 5, 6 and 7 shows the stress field for the models with 1000 m displacement considering WFS, SFS and WFW parameters. For all the figures long lines are the maximum compressive horizontal stress σ_{Hmax} and the short lines are the minimum compressive horizontal stress σ_{Hmin}. The red lines in the models show the tension and the black lines show the compression. For the "weak fault in relatively strong crust" condition, when we consider single domain model (A) the trend of σ_{Hmax} is generally NE-SW below the latitude of 40°N. But there is variation in some place like north of the 40°N latitudes it is almost E-W. And this boundary is also characterized by few NW-SE and NE-SW stress orientations. The southwestern part south of the 35°N latitudes is characterized by the N-S stress orientation (Figs. 5A, 6A and 7A). The σ_{Hmax} is compressive. Similar pattern of the stress fields were observed with decreasing displacement boundary condition, but the minimum stresses (σ_{Hmin}) with high displacement boundary conditions are tensional and the magnitude of σ_{Hmax} is large (Figs. 5, 6 and 7) compared to models with small displacements. When we consider the 3 domains models (B) (Figs. 5B, 6B and 7B) the general stress field is similar as model (A), but the magnitude of the σ_{Hmin} increases and it mainly becomes compressive and again the magnitude of the σ_{Hmin} decreases with the increasing displacement boundary condition. South of the latitudes of big bend the σ_{Hmax} is almost perpendicular to the strike of the

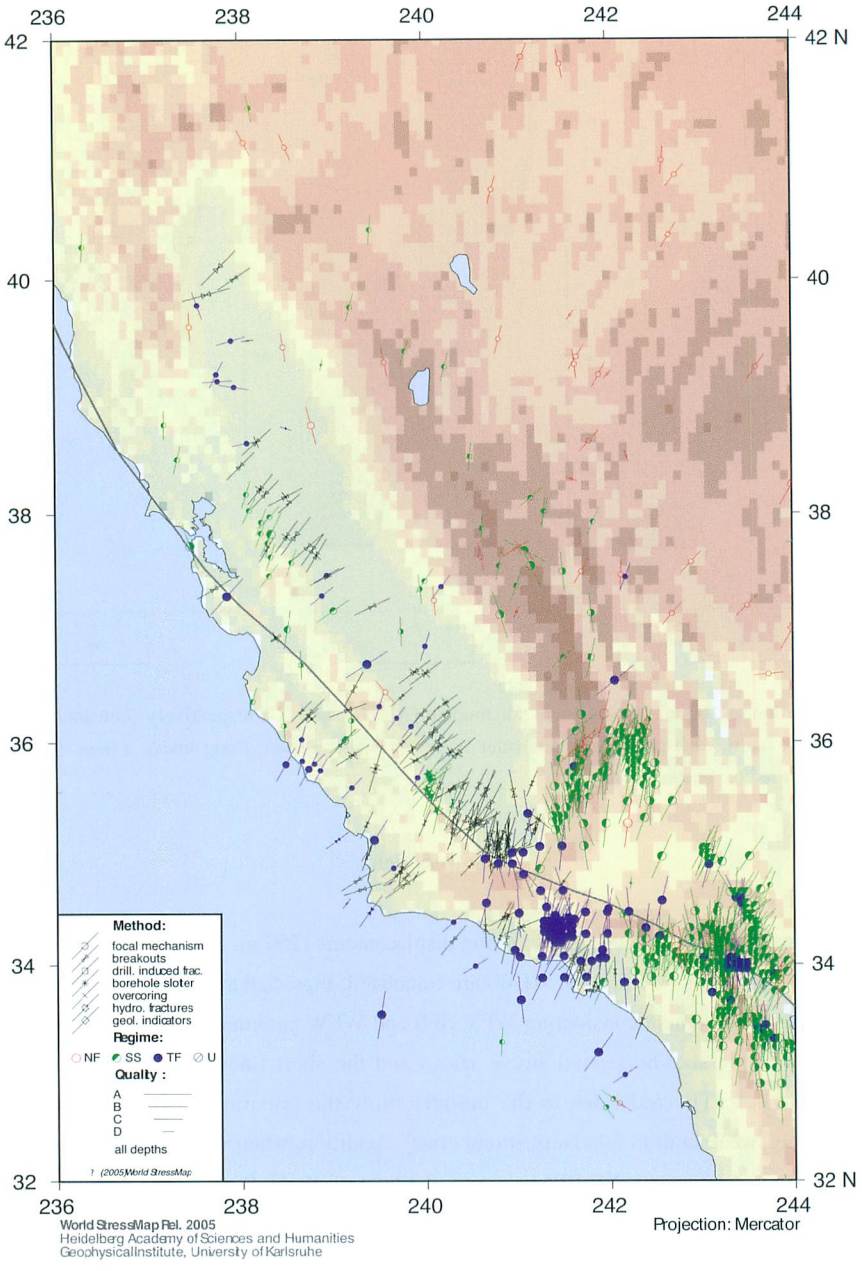

Fig. 8 Orientation of maximum horizontal stress observed in and around the modeled area (after Reinecker et al., 2005).

SAF (Figs. 5B, 6B and 7B). Considering the model (C) with the Garlock fault there is no such variation in the stress field. It is like model (B) but the stress just above the Garlock fault is now N-S.

When "SFS" is considered the tensional stress magnitude increases and propagates in more area and is clear in the figures of increasing boundary displacements (Fig. 6). The orientation of σ_{Hmax} in this condition tends to become more oblique to the trace of the San Andreas Fault.

Stress field obtained in the condition "WFW" shows, stress magnitudes decreases and there is almost no tensional stress. Stresses are oriented less obliquely to the SAF strike (Fig. 7).

Comparing with the world stress map (Fig. 8) and other stress orientation (for example Zoback and Zoback, 1980) data the calculated stress fields in our models are in good agreement. Regional stress field and σ_{Hmax} orientation in all three models are similar but model (B) shows the stress perturbation due to SAF and model (C) shows the local stress perturbation due to Garlock fault.

4.2 Displacement vector

Displacement vectors for the three models with the variation of parameters (WFS, SFS and WFW) and for the 1000 m displacements are shown in the figures 9, 10 and11 respectively. For all these figures the arrow shows the direction of motion and the length of the arrow is magnitude. In case of "WFS" (Fig. 9) the general

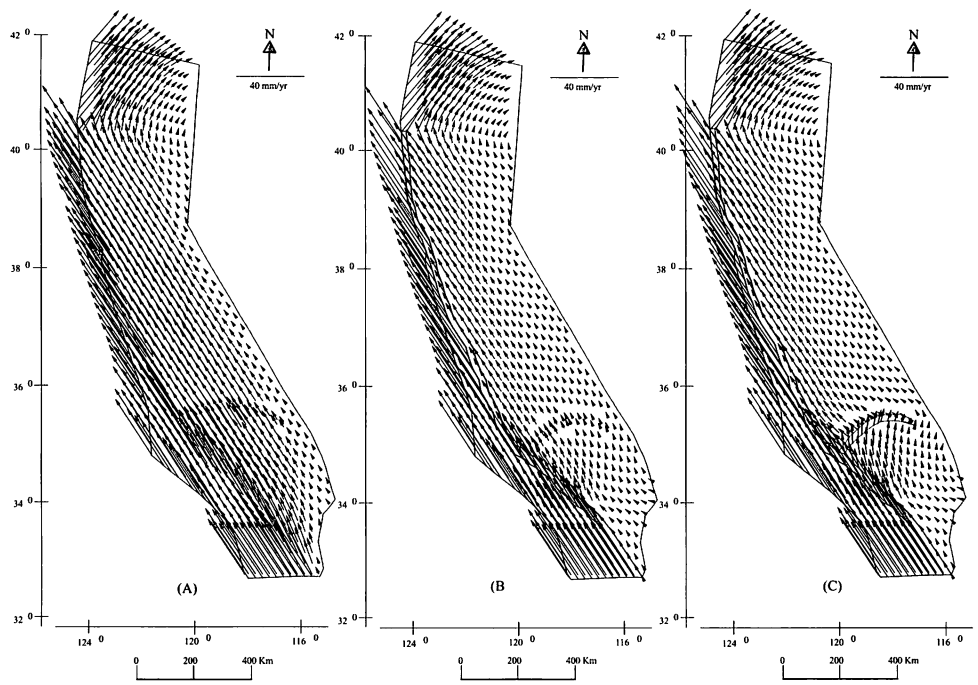

Fig. 9 Displacement vector at 1000 m displacement for model (A), (B) and (C) respectively (considering weak fault in relatively strong crust).

trend of the displacement is towards N34°W below the latitude of 40°N approximately. But between the latitude of 40°N and 42°N the displacement is towards N50°E. Decreasing the displacement boundary condition decreases the magnitude of the displacement vectors.

When we consider the three domains model (Fig. 9B) general trend is same as model (A) but south east of the big bend and south of Garlock fault the displacement vector is rotated towards north. Decreasing

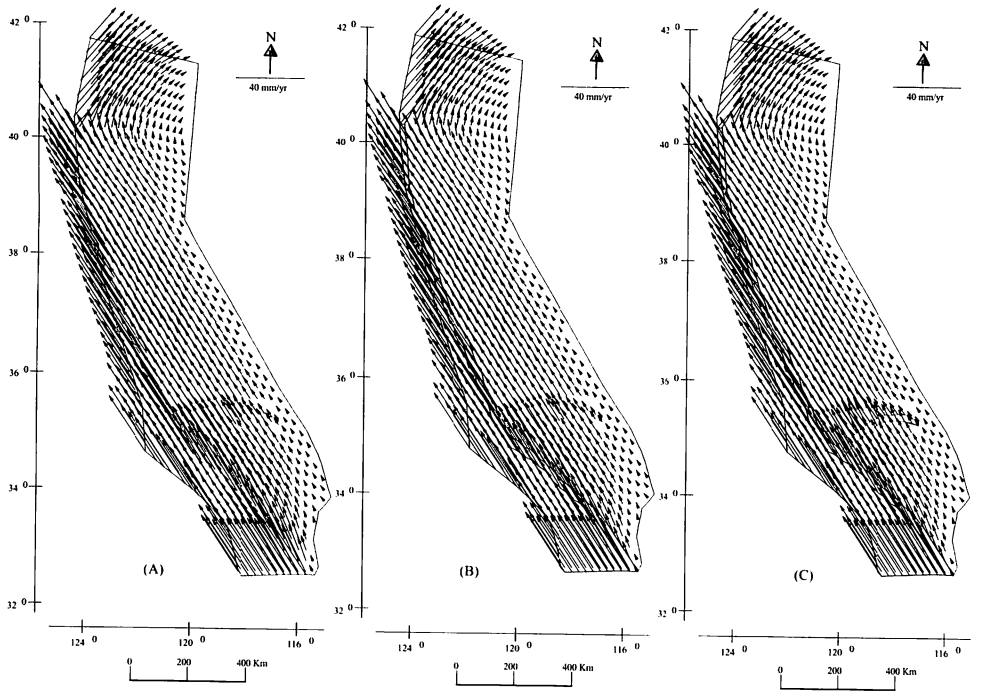

Fig.10 Displacement vector at 1000 m displacement for model (A), (B) and (C) respectively (considering strong fault in relatively strong crust).

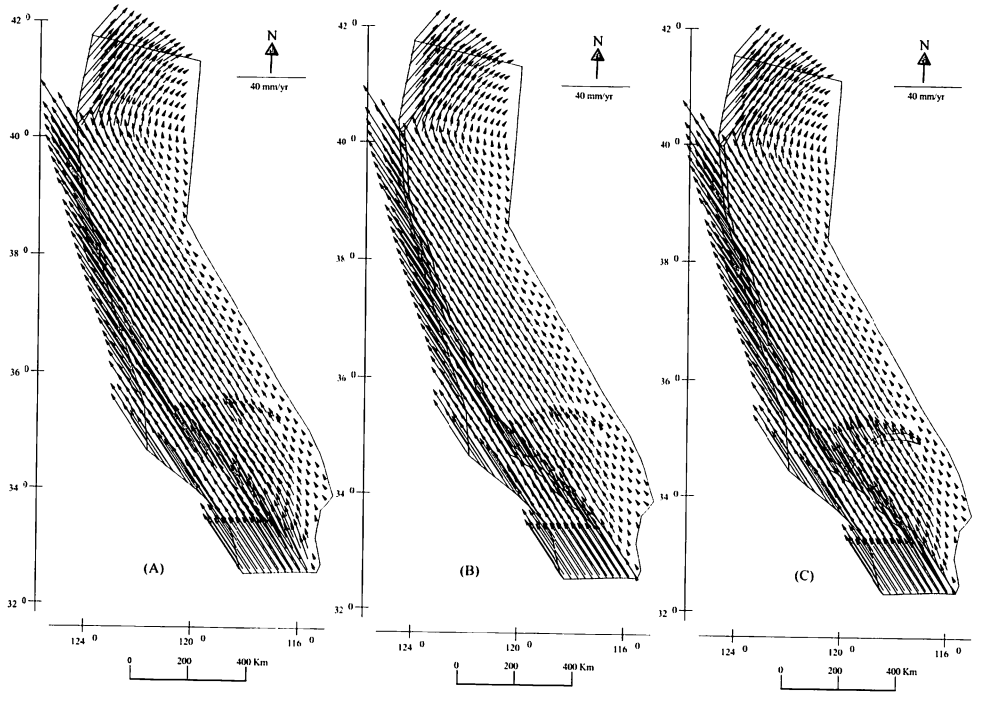

Fig.11 Displacement vector at 1000 m displacement for model (A), (B) and (C) respectively (considering weak fault in relatively weak crust).

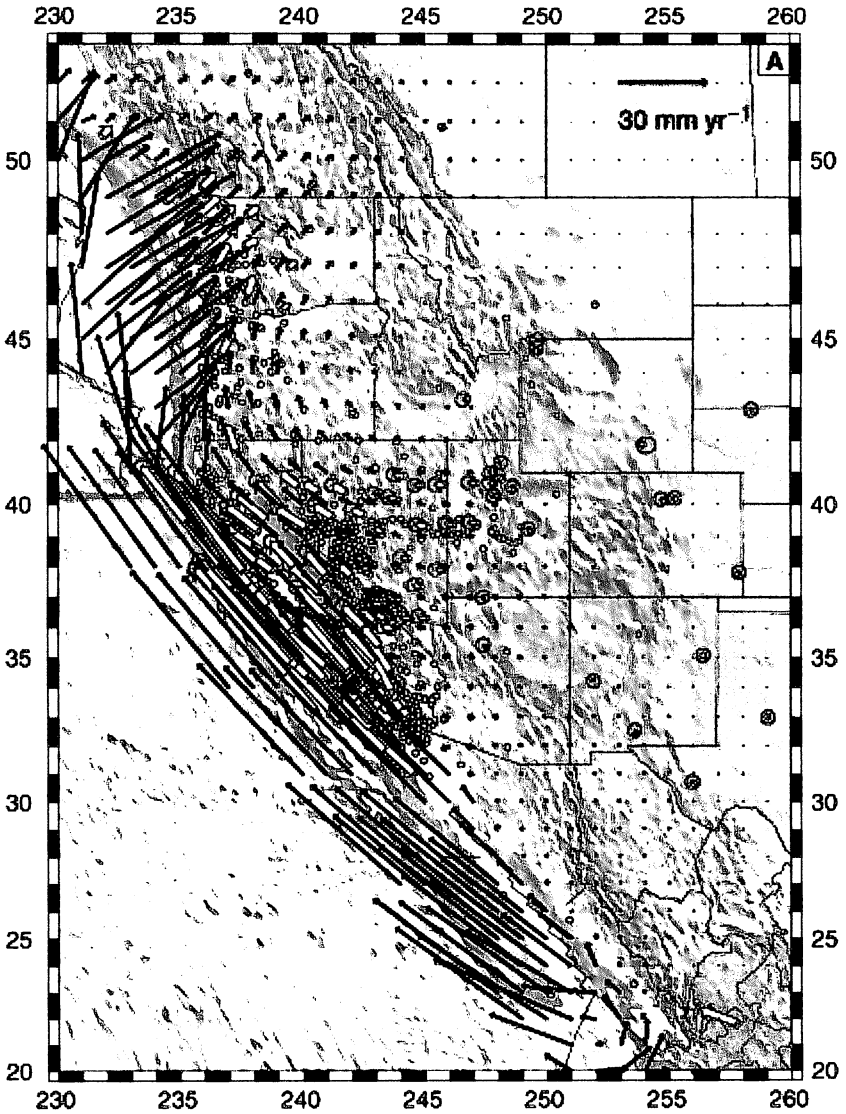

Fig.12 Continuous model velocity field (black vectors), and GPS data (white vectors) from Bennett et al. (1999) plotted relative to North American frame of reference (after Flesch et al., 2007).

displacement boundary condition decreases the magnitude of the displacement only. When we consider four domains model (C) the general trend of the displacement vector is same as in model (B) and the magnitude of the displacement vector decreases with decreasing displacement (Fig. 9C). But in the Garlock fault zone, the displacement north of the fault zone is towards the northwest and south of the fault zone towards northeast with high magnitude. So Garlock fault is simulated as a left lateral strike slip fault in our model.

Considering "SFS", the displacement vectors do not deviate in the weak fault zones and the magnitudes of the vector increases (Fig. 10).

When we consider displacement vectors of "WFW", the magnitude of displacement vector decreases and there is deviation of displacement in the weak fault zones but models with increasing displacement (Fig. 11) do not show any deviation in the weak zone.

Comparing with the velocity model and GPS velocity (Fig. 12) our calculated displacement vectors are comparable in the regional sense of movement. And in our model (B and C) of "WFS" (Fig. 9) and models with decreasing displacement in "WFW" bending of the SAF and Garlock fault has local effects on the displacement vector.

4.3 Failure analysis

Failure elements (using Byerlee's law) for the three models with parametric conditions WFS, SFS and WFW at 1000 m displacement are shown in the Figs.13, 14 and 15 respectively.

Failure elements failed under Mohr-Coulomb criterion with parametric conditions WFS for the three models with increasing displacements are shown in the Figs. 16 and 17 at 250 m and 1000 m displacements respectively. Figs. 18 and 19 show the failure elements failed under Mohr-Coulomb criterion with the parametric condition SFS at 250 m and 1000 m respectively. Similarly failure elements failed under Mohr-Coulomb criterion considering "WFW" at 1000 m are shown in the Fig. 20.

When we consider the Byerlee's law (Figs. 13, 14 and 15), in case of the single domain model (Figs. 13A, 14A and 15A) failure elements are concentrating on the northern California south of the 40°N latitude and north of the 38°N latitude as well as in the southern California south of the 34°N latitude in the eastern

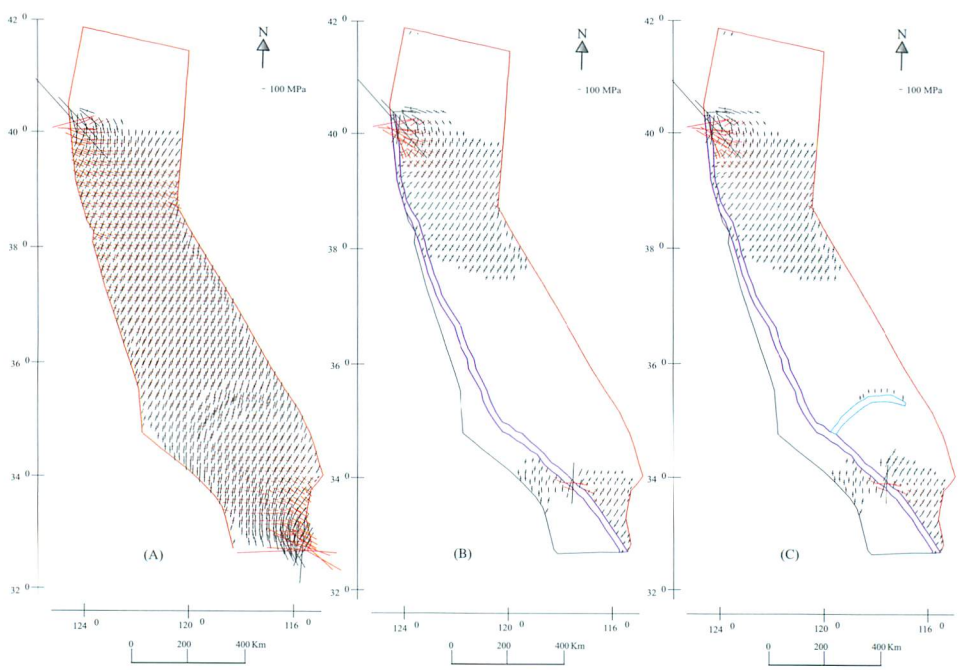

Fig.13 Failure elements at 1000 m displacement for model (A), (B), and (C) respectively using Byerlee's law (considering weak fault in the relatively strong crust), each pair of perpendicular lines represents σ_{Hmax} (long lines) σ_{Hmin} (short lines) in failure elements, and red bar shows the tension.

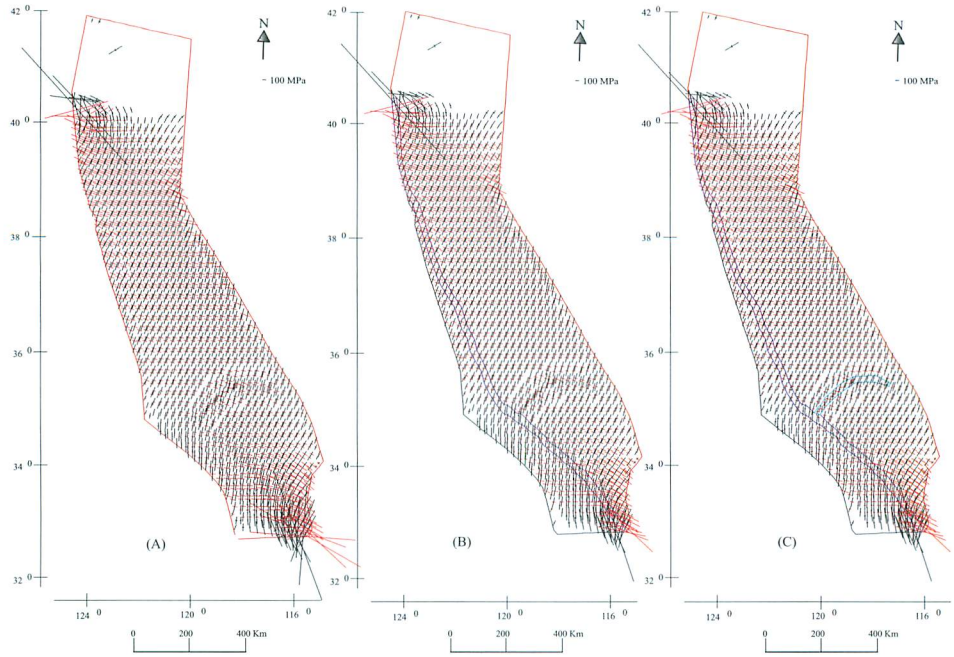

Fig. 14 Failure elements at 1000 m displacement for model (A), (B), and (C) respectively using Byerlee's law (considering strong fault in the relatively strong crust), each pair of perpendicular lines represents σ_{Hmax} (long lines) σ_{Hmin} (short lines) in failure elements, and red bar shows the tension.

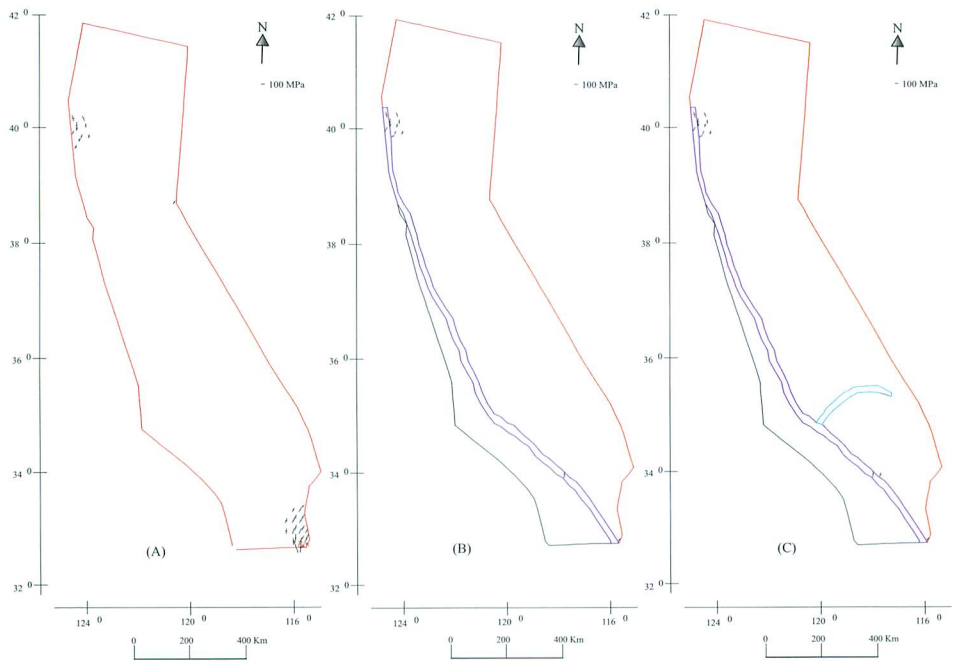

Fig. 15 Failure elements at 1000 m displacement for model (A), (B), and (C) respectively using Byerlee's law (considering weak fault in the relatively weak crust), each pair of perpendicular lines represents σ_{Hmax} (long lines) σ_{Hmin} (short lines) in failure elements, and red bar shows the tension.

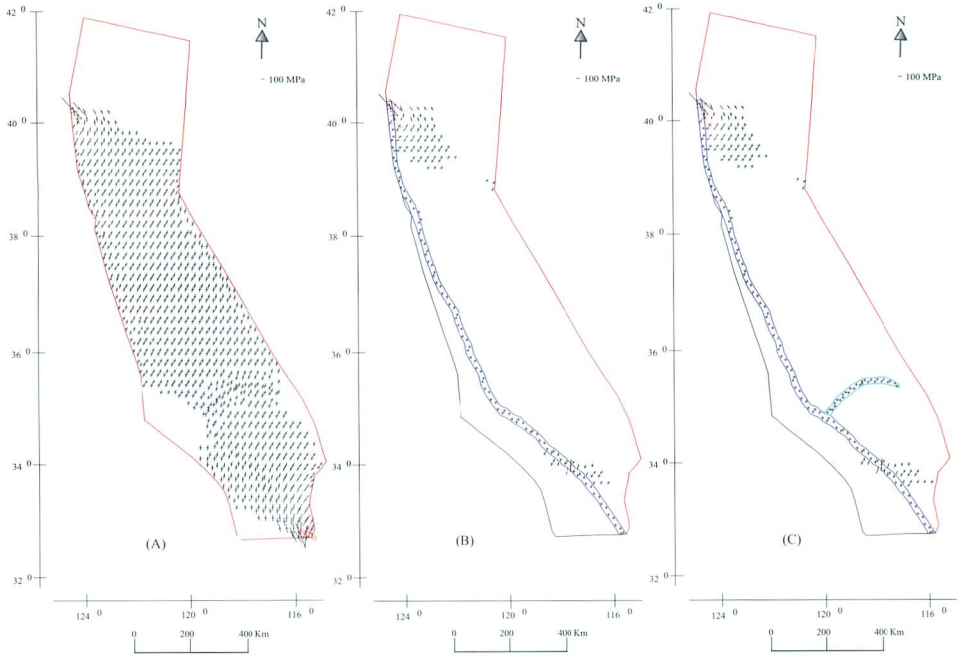

Fig.16 Failure elements at 250 m displacement for model (A), (B), and (C) respectively using Mohr-Coulomb failure criterion (considering weak fault in relatively strong crust), each pair of perpendicular lines represents σ_{Hmax} (long lines) σ_{Hmin} (short lines) in failure elements, and red bar shows the tension.

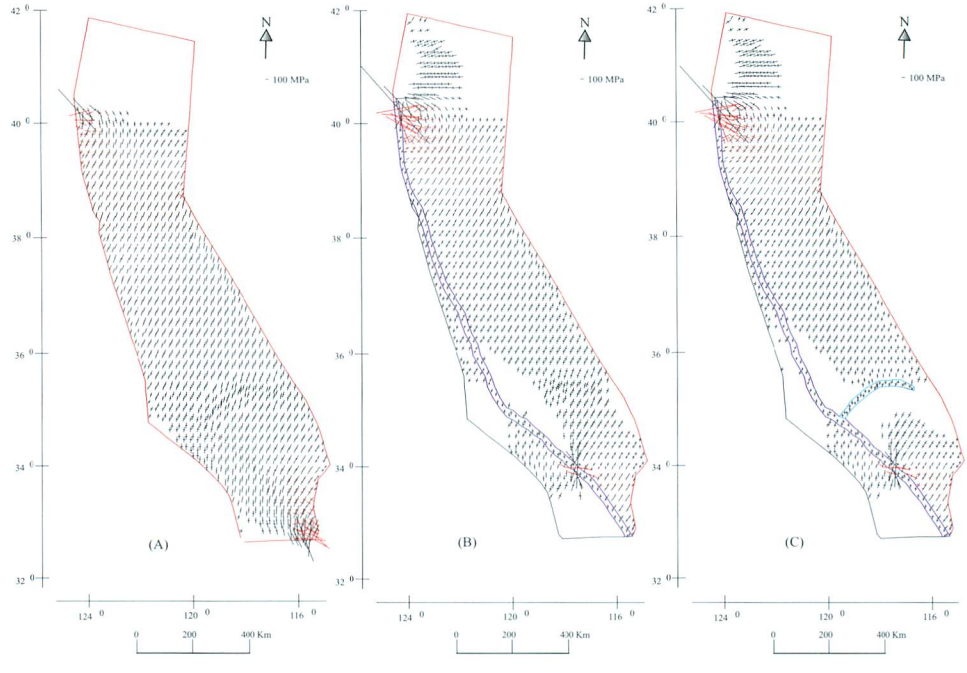

Fig.17 Failure elements at 1000 m displacement for model (A), (B), and (C) respectively using Mohr-Coulomb failure criterion (considering weak fault in relatively strong crust), each pair of perpendicular lines represents σ_{Hmax} (long lines) σ_{Hmin} (short lines) in failure elements, and red bar shows the tension.

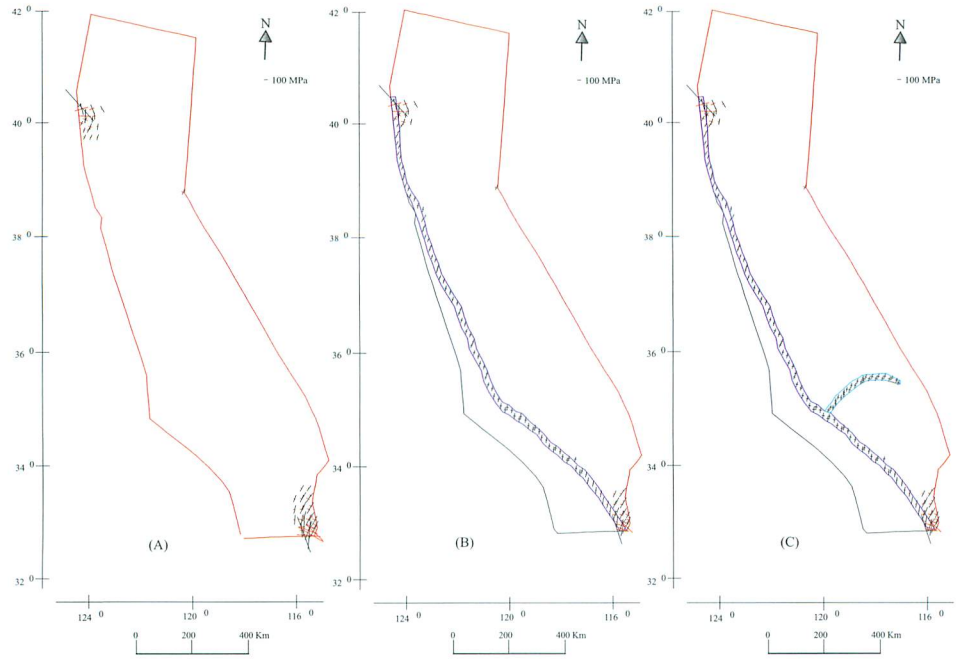

Fig.18 Failure elements at 250 m displacement for model (A), (B), and (C) respectively using Mohr-Coulomb failure criterion (considering strong fault in relatively strong crust), each pair of perpendicular lines represents σ_{Hmax} (long lines) σ_{Hmin} (short lines) in failure elements, and red bar shows the tension.

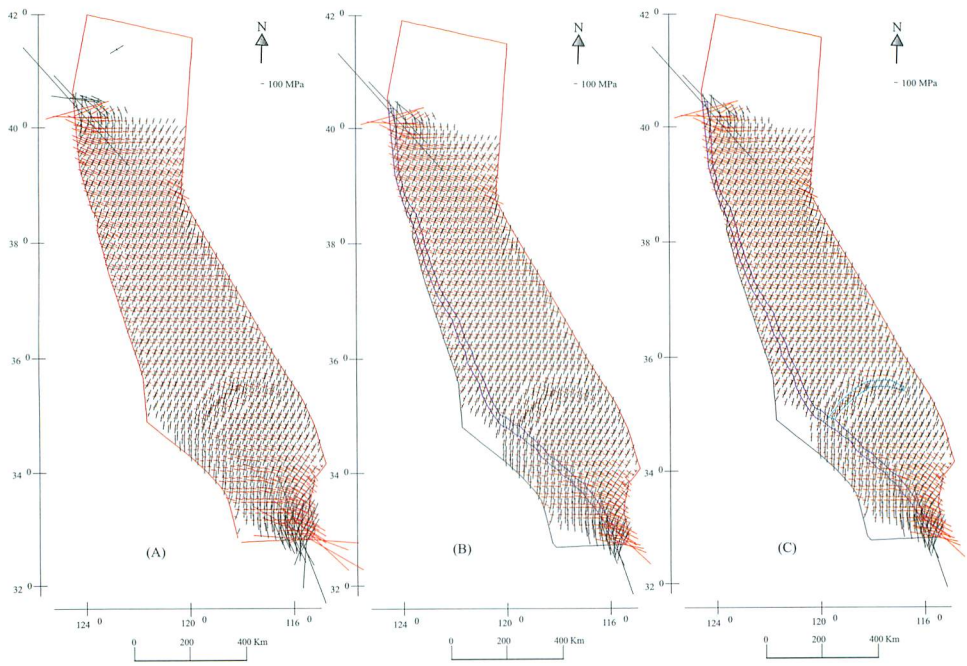

Fig. 19 Failure elements at 1000 m displacement for model (A), (B), and (C) respectively using Mohr-Coulomb failure criterion (considering strong fault in relatively strong crust), each pair of perpendicular lines represents σ_{Hmax} (long lines) σ_{Hmin} (short lines) in failure elements, and red bar shows the tension.

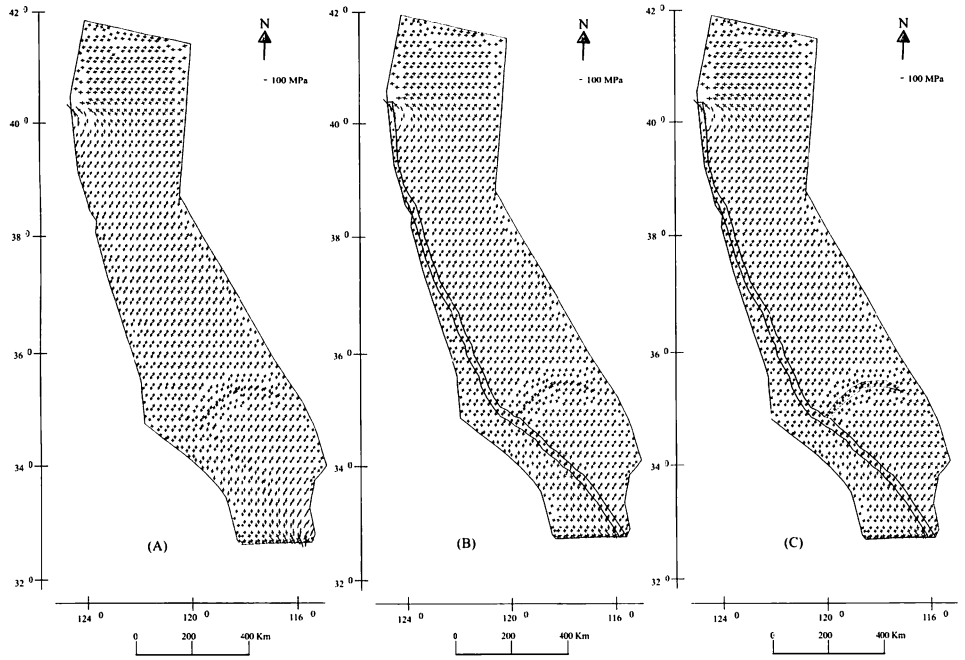

Fig.20 Failure elements at 1000 m displacement for model (A), (B), and (C) respectively using Mohr-Coulomb failure criterion (considering weak fault in relatively weak crust), each pair of perpendicular lines represents σ_{Hmax} (long lines) σ_{Hmin} (short lines) in failure elements, and red bar shows the tension.

California. High displacement boundary condition causes all the elements south of the 40°N latitudes to fail and there is increase in some tensional σ_{Hmin} (Fig 13, 14 and 15) but it is not observed when displacement boundary condition is decreased. In the case of the three and four domains models (Fig 13B, 14C, 15B, 13C, 14B and 15C) failure elements are decreased due to SAF and Garlock fault and slightly increase with increasing displacement.

When we consider Mohr-Coulomb failure criterion (Figs. 16, 17, 18, 19 and 20), in case of the single domain model (Figs. 16A, 17A, 18A, 19A and 20A) failure elements are concentrating south of the 40°N latitude, the increasing displacement slightly increases magnitude of the stress and slightly the tensional σ_{Hmin} in the northwestern side near 40°N latitudes and south eastern side near 33°N. In case of the three domains and four domains model (Figs. 16B, 18B, 16C and 18C) the failure elements are concentrated within the fault zone. But the increasing displacement boundary condition (Figs. 17B, 19B, 20B, 16C, 19C and 20C) slightly increases the magnitude of the stress and failure elements propagate out from the fault zone basically in the northern and southern California and then almost whole area.

When we consider "SFS" (Figs. 14, 18 and 19) there is increase in the failure elements out side of the fault zones and increase in σ_{Hmin} tensional. There are no such differences in the models with Byerlee's law and Mohr-Coulomb failure criterion. But the "WFW" (Fig. 15) conditions can not create failure generally and the increasing displacement boundary condition produces very few failure elements under Byerlee's law but all the elements are failed (Fig. 20) when Mohr-Coulomb criterion is used. There is very few σ_{Hmin} tensional.

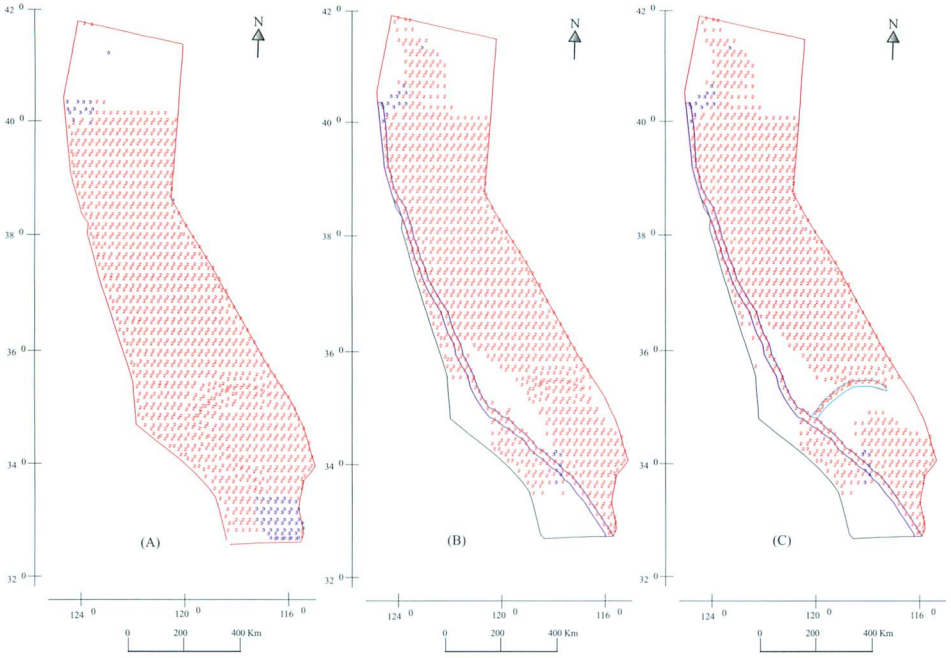

Fig.21 Fault type at 1000 m displacement for the model (A), (B) and (C) respectively for the elements failed under Mohr-Coulomb failure criterion (considering weak fault in relatively strong crust) at 12 km depth. Numbers represents failure type as 1(green) for the thrust, 2 (red) for the normal and 3 (blue) for the strike-slip.

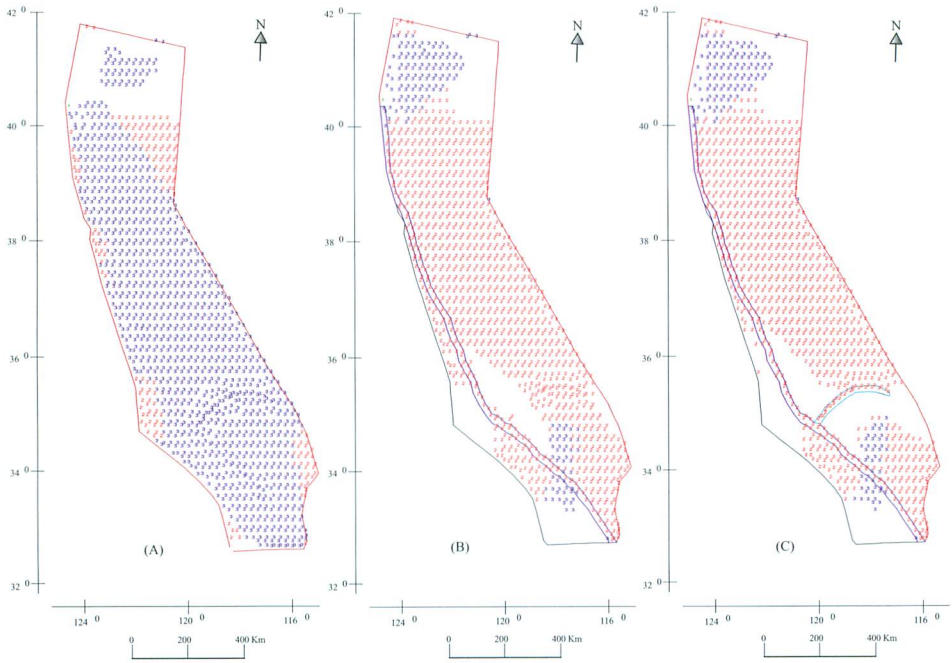

Fig.22 Fault type at 1000 m displacement for the model (A), (B) and (C) respectively for the elements failed under Mohr-Coulomb failure criterion (considering weak fault in relatively strong crust) at 4 km depth. Numbers represents failure type as 1(green) for the thrust, 2 (red) for the normal and 3 (blue) for the strike-slip.

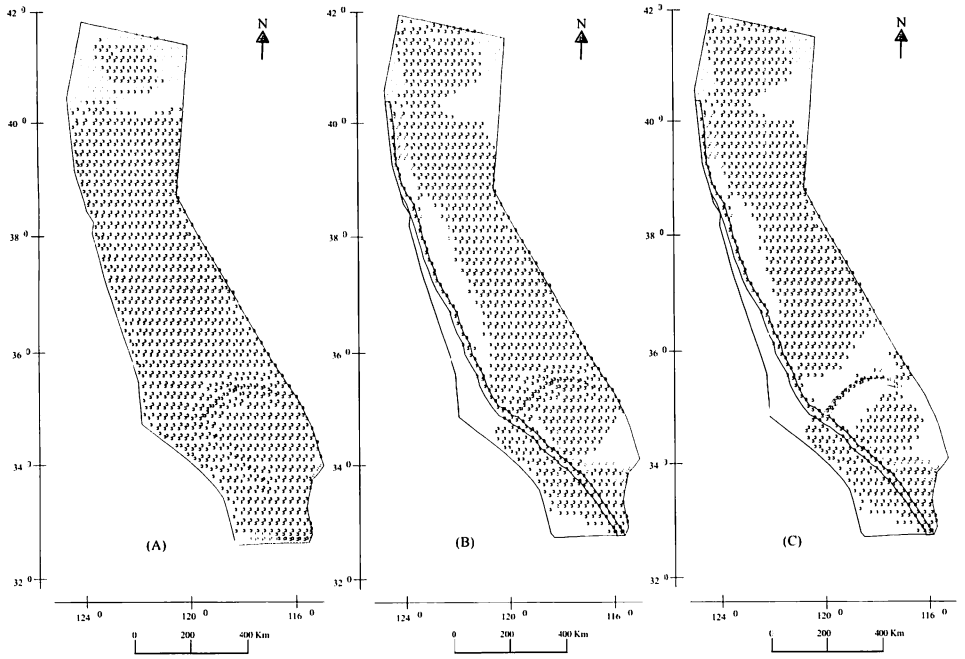

Fig.23 Fault type at 1000 m displacement for the model (A), (B) and (C) respectively for the elements failed under Mohr-Coulomb failure criterion (considering weak fault in relatively strong crust) at 0.5 km depth. Numbers represents failure type as 1(green) for the thrust, 2 (red) for the normal and 3 (blue) for the strike-slip.

Failure elements are concentrated in the fault zones in the model with Mohr-Coulomb failure criterion but not concentrated in the fault zone in the model with Byerlee's law. This deviation suggests that pre-weak zone prevents the formation of new weak zone and if the crust is strong there is probability of formation of many parallel fault zones.

4.4 Failure state and fault type

Failure state is used to analyze the fault type. As described previously, here also we use two failure criterions for the fault type analysis namely the criterions are Mohr-Coulomb failure criterion and Byerlee's law. Three states are defined and accordingly the fault types are defined as thrust, normal and strike-slip according to Anderson's theory (Hayashi, 2008).

Failure type is analyzed by varying the depth of the calculation. In this study, we use 20 km, 12 km, 8 km, 4km, 1km and 0.5 km depth. Some typical fault types are shown in the figures 21, 22 and 23 using Mohr-Coulomb failure criterion considering "WFS" parameters. These figures represent the depth wise variation of failure state (12, 4 and 0.5 km) with increasing displacement boundary conditions (1000 m) for the models (A), (B) and (C). These figures with increasing displacements and variations of depth show that at the greater depth most of the elements are failed producing the normal fault. But when the depth decreases the elements start to fail in producing the strike slip fault. Models with increasing displacements boundary conditions and

decreasing depth shows elements failed producing thrust fault in northern California coastal range and some southern part of the south California. All the models with Byerlee's law also show similar results but as seen in the failure figures there is no concentration of failure elements within fault zones.

These results shows that there is high chance of normal faulting at the depth and the same fault can act as strike slip and thrust at the shallow depth. Most of the fault at shallow depth along the SAF is strike slip but same is normal at the depth. So we conclude termination of the SAF in the depth may not be strike slip. Next if the displacement boundary condition is increased than strike slip faulting is likely to propagate towards the depth (it means there is increase in failure elements failed by strike-slip faulting in the models with increasing depth and increasing displacement) . So another conclusion drawn from this study is fault type also depends on the intensity (rate) of the tectonic forces.

5. Discussions

5.1 Model setup and limitations

Although in the nature, there is vertical and lateral variations in the rheology and the material types are inhomogeneous. The models are constructed considering the simplified homogeneous and isotropic domain properties. Elastic rheology is taken for the modeling purpose and is justifiable as 12 km is the seismogenic depth in California area. General parameters for the rock domain are taken based on the published literatures as defined earlier. There are many parallel and subparallel branches of the SAF but we consider only main strand and the biggest branch namely the Garlock fault. As the model area boundary is taken as the political boundary of the California State there may be some boundary effect due to model boundary geometry, but it seems that this effect is very less.

5.2 Stress field and maximum compressive horizontal stress (σ_{Hmax})

Many methods like borehole breakouts, focal mechanisms inversions, drill induced fractures etc are used for the calculation of the stress field especially the maximum compressive horizontal stress (σ_{Hmax}). Orientations of the maximum and minimum horizontal stress are calculated by many authors to show the differential stress in the seismogenic depth of California (Parson, 2006). The orientation of the maximum compressive horizontal stress (σ_{Hmax}) is considered as the indicator for the how much shear stress is transferring into the fault plane, and thus for the implication for the fault strength. Most of the measured stresses as shown in the world stress map (Fig. 8) and modeled data (Parson, 2006) show that orientation of the maximum horizontal stress is nearly orthogonal to the SAF along most of its length. Measured maximum principal stress direction (σ_{Hmax}) within 20 km from the fault strike on the both sides of the fault shows fault oblique compression and the far than this distance shows fault normal compression. But in our modeling, the stress orientations are more or less homogeneously oriented showing fault oblique compression favoring strong SAF. But parametrical study shows that σ_{Hmax} orientations depend on the tectonic stressing direction and do not depend on the fault and surrounding crust physical properties.

5.3 San Andreas fault and its strength

SAF strength is a subject of debate in the earth scientist community from 70's to today. Mainly there are three groups of scientists, arguing about the strength of the SAF. One group of scientists argues SAF as a weak fault in relatively strong crust (Brune et al., 1969; Mount and Suppe, 1987; Zoback et al., 1987; Lachenbruch and Sass, 1992) second group of scientists says it as a strong fault in a relatively strong crust (Scholz, 2000). And third group of scientists argues it as weak fault in relatively weak crust (Molnar, 1992). For this we tried to analyze our simulation result using Byerlee's law and Mohr- Coulomb failure criterion. Byerlee's law can be considered in support of the strong fault and variation of cohesion and friction coefficient can be utilized to check the weak fault hypothesis. The result obtained from this simulation does not directly give support to favor one hypothesis, but many calculations output like displacement vector, stress field and failure elements give secondary proof to favor weak fault in strong crust hypothesis.

5.4 Fault type

Mostly the study area lies in the strike slip regime and main strand through out its length is strike slip. Many of its parallel and sub parallel branches are also strike slip. There are also some normal and thrust faults in this area. Calculated depth dependent fault types are comparable with the observed fault type of the area only at the shallow depth. But in our model very few strike slip faults are simulated at the depth which is not comparable. All the SAF is simulated as strike slip (at shallow depth) and there are concentrations of thrust type fault in southern and northern California at shallow depth and normal fault in central California.

6. Conclusions

The results of this study allow the following conclusions. (1) As the calculated stress field and displacement vector are in good agreement with the other measured data, our imposed boundary condition has simulated the present day tectonic condition. (2) The big bend of the SAF and Garlock Fault has some local effect on the stress field as well as displacement vector and the effect of these faults and their geometry has significant effect on the failure. (3) Increasing displacement boundary condition can produce tensional stress but the σ_{Hmax} is usually compressive and oblique to the SAF but slightly vary laterally. (4) As the modeling based on the domain properties favorable for the weak fault hypothesis had simulated the present day plate kinematics, this model favor weak San Andreas in the relatively strong crust. Although the modeled stress orientation through out California is orientated oblique to the strike of the SAF somewhat favoring the strong fault in relatively strong crust hypothesis considering the alternative method for this debate (stress orientation and fault strength) (5) In the regional sense of movement, the regional stress field and displacement vectors do not deviate significantly with the implied physical parameters and strongly depends on the tectonic stressing direction, and slightly deviate with major fault geometry and local fault. (6) But the failure is relatively dependent on the geometry of the SAF and many local faults may have effect on the stress partition. (7) Depth wise variation of the fault type reveal that as the depth increases, the fault types are generally normal and

shallow depth gives more strike slip and thrust fault. So in conclusion SAF may terminate as a normal fault at the depth. (8) Another conclusion drawn from this study is combinations of physical parameter used for the fault zone and surrounding crust have strong influences on the failure pattern.

Acknowledgement

M. P. K. is grateful to Ministry of Education, Culture, Sports, Science, and Technology, (Monbukagakusho) Japan for the scholarship to carry out this research work under the special graduate program of the Graduate School of Engineering and Science, University of the Ryukyus, Okinawa, Japan.

References

Argus, D.F. and Gordon R.G., 2001. Present tectonic motion across the Coast Ranges and the San Andreas fault system in central California. Geological Society of America Bulletin, 113, 1580-1592.

Atwater, T., 1970. Implications of plate tectonics for the Cenozoic tectonic evolution of western North America. Geological Society of America Bulletin, 81, 3513-3635.

Bird P. and Kong X., 1994. Computer simulations of California tectonics conform very low strength of major fault. Geological Society of America Bulletin, 106, 159-174.

Brune, J.N., Henyey, T.L. and Roy, R.F., 1969. Heat flow, stress and rate of slip along the San Andreas fault, California. Journal of Geophysical Research, 74, 3821-3827.

Cai, Y., and Wang C.Y., 2001. Testing fault models with numerical simulation: example from central California. Tectonophysics, 343, 233-238.

Chery J., Zoback M.D. and Hassani R., 2001. An integrated mechanical model of the San Andreas fault in central and northern California. Journal of Geophysical Research, 106, 22,051-22,066.

Crowell, J.C., 1952. Probable large lateral displacement on San Gabriel Fault, southern California. American Association of Petroleum Geologist Bulletin, 36, 2026 - 2035.

d'Alessio, M.A., Johanson, I.A., Burgmann, R., Schmidt, D.A. and Murray, M.H., 2005. Slicing up the San Francisco Bay Area: Block kinematics and fault slip rate from GPS-derived surface velocities. Journal of Geophysical Research, 110(B06403), 1-19. doi: 10.1029/2004JB003496.

DeMets, C., Gordon, R.G., Argus, D.F. and Stein, S., 1994. Effects of recent revisions to the geomagnetic reversal time scale on estimates of current plate motions, Geophysical. Research Letters, 21, 2191-2194.

Flesch, L.M., Holt, W.E., Haines, A.J., Wen, L., Shen-Tu B., 2007. The dynamics of western North America: stress magnitudes and the relative role of gravitational potential energy, plate interaction at the boundary and basal tractions. Geophysical Journal International 169, 866?896. doi: 10.1111/j.1365-246X.2007.03274.x.

Fuis, G.S., Mooney, W.D., 1990. Lithospheric structure and tectonics from seismic-refraction and other data. in R. E. Wallace, ed., The San Andreas Fault System: U. S. Geological Survey Professional Paper 1515, 207-236.

Hayashi D., 2008. Theoretical basis of FE simulation software package. Bull. Fac. Sci. Univ. Ryukyus, No. 85,

81-95. http://ir.lib.u-ryukyu.ac.jp/

Irwin, W.P. 1990. Geology and Plate-Tectonic Development. in R. E. Wallace, ed., The San Andreas Fault System: U. S. Geological Survey Professional Paper 1515, 61-80.

Lachenbruch, A.H. and Sass, J.H., 1992. Heat flow from Cajon Pass, fault strength, and tectonic implications. Journal of Geophysical Research, 97, 4995-5015.

Lynch, J.C., and Richards M.A., 2001. Finite elements models of the stress orientations in well-developed strike-slip fault zones: Implications for the distribution for lower crustal strain. Journal of Geophysical Research, 106, 26,707-26,729.

Malservisi, R., Gans C. and Furlong K.P., 2003. Numerical modeling of strike-slip creeping faults and implications for the Heyward fault, California. Tectonophysics 361, 121-137.

Minster, J.B. and Jordan, T.H., 1978, Present-day plate motions. Journal of Geophysical Research, 83, 5331-6354.

Molnar, P., 1992. Brace-Goetze Strength Profiles, The Partitioning of Strike-slip and Thrust Faulting at Zones of Oblique Convergence, and the Stress-Heat Flow Paradox of the San Andreas Fault, in Evans, B. & Wong, T. F. eds., Fault Mechanics and Transport Properties of Rocks: Academic, London, 435?459.

Mount, V.S. and Suppe, J., 1987. State of stress near the San Andreas fault: Implications for wrench tectonics. Geology, 15, 1143-1146.

Noson, L.L., Qamar, A. and Thorsen, G. W., 1988. Washington State Earthquake Hazards. Washington State Department of Natural Resources, Washington Division of Geology and Earth Resources Information Circular 85. http://www.pnsn.org/INFO_GENERAL/NQT/welcome.html

Parsons, T. 2006. Tectonic stressing in California modeled from GPS observations. Journal of Geophysical Research, 111(B03407), 1-16. doi: 10.1029/2005JB003946.

Powell, R.E. and Weldon, R.J. 1992. Evolution of the San-Andreas Fault. Annual Review of Earth and Planetary Sciences, 20, 431-468.

Reinecker, J., Heidbach, O., Tingay, M., Sperner, B. and Muller, B. 2005. The 2005 release of the World Stress Map. www.world-stress-map.org

Savage, J.C., Gan, W. Prescott, W.H. and Svarc J.L., 2004. Strain accumulation across the Coast Ranges at the latitude of San Francisco, 1994-2000, Journal of Geophysical Research, 109(B03413), 1-11. doi: 10.1029/2003JB002612.

Scholz, C. H., 2000. Evidence for a strong San Andreas fault. Geology 28, 163-166.

Swanson D.A., Cameron K.A., Evarts R.C., Pringle P.T. and Vance J.A., 1989. Cenozoic Volcanism in the Cascade Range and Columbia Plateau, Southern Washington, and Northernmost Oregon: AGU Field Trip Guidebook T106. http://vulcan.wr.usgs.gov/Volcanoes/PacificNW/AGUT106/hood.html#mounthood

Wallace, R.E., 1990. General Features and Geomorphic Expression. in R. E. Wallace, ed., The San Andreas Fault System, U. S. Geological Survey Professional Paper 1515, 3-21.

Wood, C.A. and Kienle, J., 1990. Volcanoes of North America: U.S. and Canada. Cambridge University Press, 354 p. ISBN 052143811X, 9780521438117.

Zoback, M.D., Zoback, M.L., Mount, V.S., Suppe, J., Eaton, J.P., Healy J.H., Oppenheimer, D., Reasenberg, P., Jones, L., Raleigh, C.B., Wong, I.G., Scotti, O. and Wentworth, C., 1987. New evidence on the state

of stress of the San Andreas fault system. Science, 238, 1105-1111.

Zoback, M.L. and Zoback, M. D., 1980. State of stress in the conterminous United States. Journal of Geophysical Research, 85, 6113-6156.